

PROBING NON-GAUSSIANITIES ON LARGE SCALES IN WMAP5 AND WMAP7 DATA USING SURROGATES

C. RÄTH¹, G. ROSSMANITH¹, G. E. MORFILL¹, A. J. BANDAY^{2,3}, K. M. GÓRSKI^{4,5}

¹*Max-Planck-Institut für extraterrestrische Physik, Giessenbachstr. 1, 85748 Garching, Germany*

²*Centre d'Etude Spatiale des Rayonnements, 9, Av du Colonel Roche, 31028 Toulouse, France*

³*Max-Planck-Institut für Astrophysik, Karl-Schwarzschild-Str. 1, 85741 Garching, Germany*

⁴*Jet Propulsion Laboratory, California Institute of Technology, Pasadena, CA 91109, USA*

⁵*Warsaw University Observatory, Aleje Ujazdowskie 4, 00 - 478 Warszawa, Poland*

Probing Gaussianity represents one of the key questions in modern cosmology, because it allows to discriminate between different models of inflation. We test for large-scale non-Gaussianities in the cosmic microwave background (CMB) in a model-independent way. To this end, so-called first and second order surrogates are generated by first shuffling the Fourier phases belonging to the scales not of interest and then shuffling the remaining phases for the length scales under study. Using scaling indices as test statistics we find highly significant signatures for both non-Gaussianities and asymmetries on large scales for the WMAP data of the CMB. We find remarkably similar results when analyzing different ILC-maps based on the WMAP five and seven year data. Such features being independent from the map-making procedure would disfavor the fundamental principle of isotropy as well as canonical single-field slow-roll inflation - unless there is some undiscovered systematic error in the collection or reduction of the CMB data or yet unknown foreground contributions.

1 Introduction

One of the key questions in cosmology is to probe the Gaussianity of the primordial density fluctuations, because it allows to discriminate between different models of inflation. While the simplest model of inflation, namely single-field slow-roll inflation¹, predicts that the temperature fluctuations of the cosmic microwave background (CMB) correspond to a (nearly) Gaussian, homogeneous, and isotropic random field, more complex models may give rise to non-Gaussianity (NG). Models in which the Lagrangian is a general function of the inflaton and powers of its first derivative can lead to scale-dependent non-Gaussianities, if the sound speed varies during inflation^{2,3}. Similarly, string theory models that give rise to large non-Gaussianity have a natural scale dependence⁴. Possible deviations from Gaussianity have been investigated in studies based on e.g. the WMAP data of the CMB (see e.g. Komatsu et al.⁵ and references therein) and claims for the detection of non-Gaussianities and other anomalies, like hemispherical power asymmetry, the 'axis of evil', the Cold Spot etc. have been made. However, most of the tests on non-Gaussianities do not take into account any possible scale-dependency. In this contribution we apply the formalism of surrogate data sets, which was recently adapted to CMB data analysis⁹, to test for non-Gaussianities on large scales in the WMAP data. Special emphasis is put on a comparison of the WMAP five year data with the WMAP seven year data.

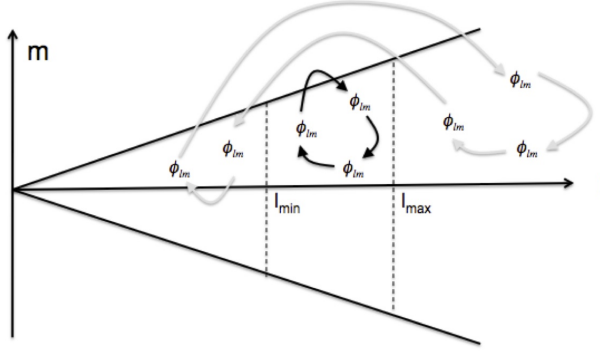


Figure 1: Schematic view of the shuffling procedure on the l - m -plane for generating the first and second order surrogates. The gray arrows indicate the phase permutations for obtaining first order surrogates and the black arrows show the shuffling for making the second order surrogates.

2 Data Sets

We use the foreground-cleaned Internal Linear Combination (ILC) maps generated and provided by the WMAP-team on the basis of the five year (WMAP5)⁶ and seven year (WMAP7)⁷ data. For comparison we also analysed the five year ILC-map (NILC5) produced by Delabrouille et al.⁸, which was generated pursuing a needlet-based approach for removing the foreground contributions.

3 Surrogates and Scaling Indices

The model-independent test for scale-dependent non-Gaussianities is based on the use of so-called surrogate data sets. As test statistics for NGs we use scaling indices. Both methods were introduced and described in detail previously^{9,10,11}. Here, we briefly review the main points of the two formalisms.

3.1 Surrogates

Consider a CMB map $T(\theta, \phi)$, where $T(\theta, \phi)$ is Gaussian distributed, which can easily be achieved by a rank-ordered remapping of the temperatures onto a Gaussian distribution. We calculate the Fourier transform of $T(\theta, \phi)$. The complex valued coefficients a_{lm} , $a_{lm} = \int d\Omega_n T(n) Y_{lm}^*(n)$ can be written as $a_{lm} = |a_{lm}| e^{i\phi_{lm}}$ with $\phi_{lm} = \arctan(Im(a_{lm})/Re(a_{lm}))$. The linear or Gaussian properties of the underlying random field are contained in the absolute values $|a_{lm}|$, whereas all higher order correlations (HOCs) – if present – are encoded in the phases ϕ_{lm} and the correlations among them. To ensure that the distribution of the phases is uniform, we also perform a rank ordered remapping of the phases ϕ_{lm} . To test for scale-dependent NGs we first generate a first order surrogate map, in which any phase correlations for the scales, which are not of interest (here: the small scales), are randomized. This is achieved by a random shuffle of the phases ϕ_{lm} for $l > l_{cut}, 0 < m \leq l$, where $l_{cut} = 20$ throughout this study and by performing an inverse Fourier transformation. Second, N (here: $N = 500$) realizations of second order surrogate maps are generated for the first order surrogate map, in which the remaining phases ϕ_{lm} with $1 < l \leq l_{cut}, 0 < m \leq l$ are shuffled while the already randomized phases for the small scales are preserved. In Fig. 1 the phase shuffling procedure for generating first and second order surrogates is schematically visualized.

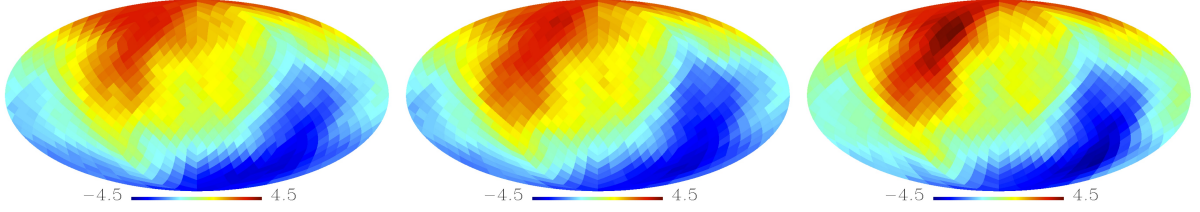


Figure 2: Deviation S as derived from rotated upper hemispheres for $\langle\alpha(r_{10})\rangle$ for the WMAP5 ILC map (left), the WMAP7 ILC map (middle) and the needlet-based ILC map (right).

3.2 Scaling Indices

To compare the two classes of surrogates, we calculate local statistics in the spatial domain, namely scaling indices (SIM) as described previously^{10,11}. In brief, scaling indices estimate local scaling properties of a point set P . The spherical CMB data can be represented as a three-dimensional point distribution $P = \vec{p}_i = (x_i, y_i, z_i), i = 1, \dots, N_{pixels}$ by transforming the temperature fluctuations into a radial jitter. For each point \vec{p}_i the local weighted cumulative point distribution ρ is calculated $\rho(\vec{p}_i, r) = \sum_{j=1}^{N_{pixels}} e^{-(\frac{d_{ij}}{r})^2}$ with $d_{ij} = \|\vec{p}_i - \vec{p}_j\|$. The weighted scaling indices $\alpha(\vec{p}_i, r)$ are then obtained by calculating the logarithmic derivative of $\rho(\vec{p}_i, r)$ with respect to r , $\alpha(\vec{p}_i, r) = \frac{\partial \log \rho(\vec{p}_i, r)}{\partial \log r}$. Using the above-given expression for the local weighted cumulative point distribution ρ , the following analytical formula for the scaling index α

$$\alpha(\vec{p}_i, r) = \frac{\sum_{j=1}^N 2(\frac{d_{ij}}{r})^2 e^{-(\frac{d_{ij}}{r})^2}}{\sum_{j=1}^N e^{-(\frac{d_{ij}}{r})^2}} \quad (1)$$

is obtained. For each pixel we calculated scaling indices for ten different scales, $r_1 = 0.025, \dots, r_{10} = 0.25$ in the notation of R ath et al.¹⁰.

4 Results

For each scale we calculate the mean ($\langle\alpha\rangle$) of the scaling indices $\alpha(\vec{p}_i, r)$ derived from a set of pixels belonging to rotated hemispheres. The differences of the two classes of surrogates are then quantified by the σ -normalised deviation $S(Y) = (Y_{surro1} - \langle Y_{surro2} \rangle) / \sigma_{Y_{surro2}}$, $Y = \langle \alpha(\vec{p}_i, r_j) \rangle$, $j = 1, \dots, 10$, surro1: first order surrogate, surro2: second order surrogate. Fig. 2 shows the deviation $S(\langle\alpha(r_{10})\rangle)$ as derived from pixels belonging to the respective upper hemispheres for 768 rotated reference frames for the three ILC-maps under study. The z-axis of the respective rotated reference frame pierces the center of the respective colour-coded pixel.

Statistically significant signatures for non-Gaussianity and ecliptic hemispherical asymmetries become immediately obvious, whereby the patterns of asymmetry remain remarkably similar for the three maps. Interestingly enough, we obtain slightly larger deviations for the WMAP7 map ($S_{min} = -3.99$, $S_{max} = 3.73$) as compared to the WMAP5 map ($S_{min} = -3.87$, $S_{max} = 3.51$). We find the largest deviation ($S_{min} = -4.36$, $S_{max} = 4.5$) for the NILC map, which can be considered as a more precise full-sky CMB temperature map than the ILC maps generated by the WMAP team⁸. Thus, the level of non-Gaussianity systematically increases, when the underlying CMB-map becomes less noisy and less foreground contaminated.

To quantify the similarity of the patterns of asymmetry in the three maps we calculate the cross-correlation $C(r)$ of the $S(Y)$ -maps derived from the three input maps as a function of the scaling range r . The results are shown in fig. 3 (left). For each scaling range r the three maps are highly correlated among each other with $C(r)$ always being larger than 0.87. The highest correlations are found for the largest scales r , where $C(r)$ reaches values of 0.98 and more. Thus,

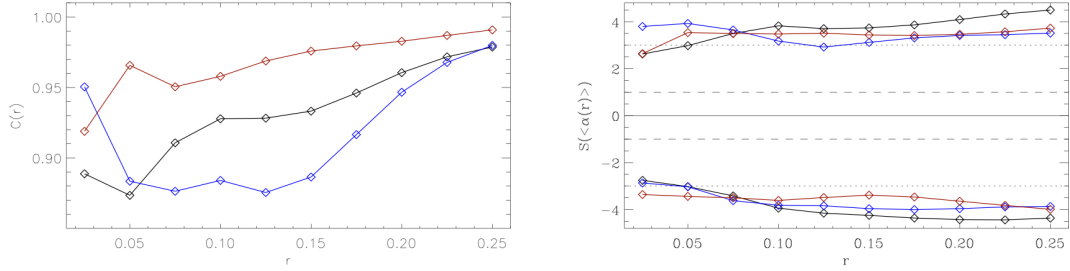


Figure 3: Left side: Cross correlation coefficient $C(r)$ for the $S(Y)$ -maps as a function of the scaling range r . Black: NILC vs. WMAP5, blue: NILC vs. WMAP7 and red: WMAP5 vs. WMAP7. Right side: Minimal and maximal values of the σ -normalized deviations $S(Y)$ for the rotated hemispheres for each scaling range r . Black: NILC, blue: WMAP5 and red: WMAP7.

on all scales r the patterns of asymmetry are very similar for each input map. On the right hand side of fig. 3 we show the minimum and maximum of S as a function of r . Except for the smallest r 's we obtain for each map stable 3σ -deviations for both extrema, where – once again – the NILC map always yields the largest deviations for scaling ranges $r > 0.1$.

5 Conclusions

In conclusion, we detect highly significant signatures for asymmetries and non-Gaussianities for large scales ($l < 20$) in the WMAP five and seven year data. The increase of the signal with decreasing noise as well as the very high correlations between the significance maps points towards an intrinsic nature of the detected anomalies, which are independent of the map making procedure. Such features would disfavor the fundamental principle of isotropy as well as canonical single-field slow-roll inflation - unless there is some undiscovered systematic error in the collection or reduction of the CMB data or yet unknown foreground contributions. Thus, further tests are required to rule out other systematic effects as origin of the detected anomalies.

Acknowledgments

Many of the results in this contribution have been obtained using HEALPix¹². We acknowledge the use of LAMBDA. Support for LAMBDA is provided by the NASA Office of Space Science. Finally, CR would like to thank the organisers for a very enjoyable meeting.

References

1. A. H. Guth, *Phys. Rev. D* **23**, 347 (1981).
2. C. Armendariz-Picon, T. Damour and V. Mukhanov, *Physics Letters B* **458**, 209 (1999).
3. J. Garriga and V. Mukhanov, *Physics Letters B* **458**, 219 (1999).
4. M. Lo Verde *et al.*, *Journal of Cosmology and Astro-Particle Physics* **4**, 14 (2008).
5. E. Komatsu *et al.*, *Astrophys. J. Suppl. Ser.* **180**, 330 (2009).
6. B. Gold *et al.*, *Astrophys. J. Suppl. Ser.* **180**, 265 (2009).
7. B. Gold *et al.*, arXiv:1001.4555.
8. J. Delabrouille *et al.*, *Astron. & Astrophys.* **493**, 835 (2009).
9. C. Räth *et al.*, *Phys. Rev. Lett.* **102**, 131301 (2009).
10. C. Räth, P. Schuecker and A. J. Banday, *Mon. Not. R. Astron. Soc.* **380**, 466 (2007).
11. G. Rossmanith *et al.*, *Mon. Not. R. Astron. Soc.* **399**, 1921 (2009).
12. K. M. Górski *et al.*, *Astrophys. J.* **622**, 759 (2005).